CONTENTS

Simultaneous, Independent Control of Many Actuators With a Clinical MRI Scanner

Aaron Becker, Ouajdi Felfoul, and Pierre Dupont

***Abstract*— Actuators that are powered, imaged, and controlled by Magnetic Resonance (MR) scanners offer the potential of inexpensively providing wireless control of MR-guided robots. Similar to traditional electric motors, the MR scanner acts as the stator and generates propulsive torques on an actuator rotor containing one or more ferrous particles. The MR scanner can control three orthogonal gradient fields. Prior work demonstrated control of a single actuator rotor. This paper proposes and demonstrates independent, simultaneous control of n rotors. Our method relies on inhomogeneity between rotors, such as insuring no rotor axes are parallel. We provide an easily-implemented control law with global asymptotic convergence, velocity and position controllers, optimization techniques for implementation, and a hardware demonstration. Code for simulations and control laws is available online.**

Is it $\mathbf{M}_s$ or $\mathbf{M}_{s_z}$?

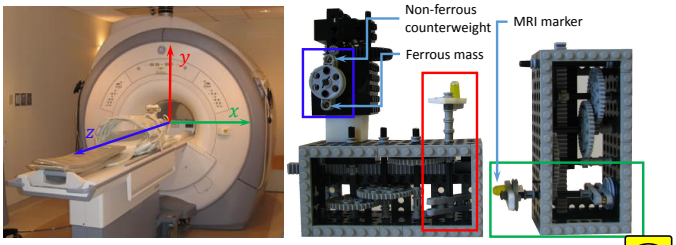

Fig. 1. Three orthogonal rotors that can be independently actuated by the same magnetic gradient field. In this paper we prove that n non-parallel rotors can be simultaneously controlled. The torque from these rotors could power multi-DOF robotic actuators running untethered inside an MRI bore.
Insert new images, add $\mathbf{a_i}$

I. Introduction

Our goals are to create transformative robotic technology that uses Magnetic Resonance Imaging (MRI) systems to power, control, and image robots under the guidance and control of a clinician. This tetherless robot technology has broad applications in medicine and biology and addresses current needs for small, low-cost medical robots. MRI-powered actuators can be used to power small MRI-compatible robots for performing ultra-minimally invasive surgery.

Our efforts are organized around three specific tasks:

1) create design principles for MRI-powered actuators
2) develop motion planning and control algorithms for MRI-powered robots
3) design MRI pulse sequences for closed-loop robot control

This research is an initial step toward a robotic technology platform that can be functionalized to perform a host of diagnostic and therapeutic tasks. Given the widespread availability of MRI scanners, dissemination of the technology could be rapid and inexpensive, involving only a software upgrade. Furthermore, robots constructed using this technology could be low cost and potentially disposable.

A. Advantages of MRI

Ultra-minimally invasive robots with an external footprint on the order of 10 cm would provide incredible benefits with respect to the current generation of surgical robots. These benefits include smaller incisions resulting in less damage and trauma to healthy tissue as well as substantial reductions in cost. Furthermore, robots of this size could fit inside an MR scanner to take advantage of its superior soft tissue imaging. MRI offers methods for a comprehensive diagnosis and characterization of tissue pathophysiology, as well as the delineation of targets for biopsies and therapeutic interventions. In addition, the improved MRI frame rates achieved in recent years [1] would facilitate many new types of interventions performed under real-time robot guidance

B. Advantages of MR Motors

The importance of robotically-assisted MR-guided interventions is well recognized by the clinical and research communities [4]. The development of MR-compatible robotic systems has faced several challenges, however, related to compatibility and space constraints. The actuators must ensure MRI safety, preserve image quality, and be able to operate unaffected by the scanner's electrical and magnetic fields. Several groups worldwide have developed MR-compatible robotics systems [3-8] [2]. These systems are usually specific to the prostate, breast, or brain and most perform the task of needle guidance for biopsies or interventional therapies.

For compatibility, alternative actuation principles are employed, such as Ultrasonic, pneumatic . . .

C. Overview of Methodology

The gradient field produced within an MRI is produced by three orthogonal sets of coil pairs that together can produce a uniform gradient field. The three coil pairs are independently controlled. The magnetic field generated is applied along the entire bore of the scanner, so multiple rotors can simultaneously harvest this power.

Seminal work from our lab designed a single-DOF MRI-powered actuator for use as a tetherless biopsy robot [3].

A. Becker, O. Felfoul, and P. Dupont are with the Department of Cardiovascular Surgery, Boston Children's Hospital and Harvard Medical School, Boston, MA, 02115 USA first name.lastname@childrens.harvard.edu,

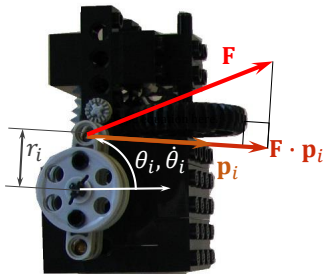

Fig. 2. MRI-powered, single-DOF actuator. Angular position and velocity $[\theta_i, \dot{\theta}_i]^\intercal$. The torque on rotor is the magnetic force projected to a vector tangent to the ferrous sphere's positive direction of motion, $r_i \mathbf{F} \cdot \mathbf{p}_i(t)$
Insert new image

This was extended to closed-loop control of a single rotor in [4].

Our paper extends previous work to control multiple rotors, and is organized as follows. We describe our model and control law in Section II. Section III examines how to optimize system design. We report the results of our experiments in Section IV, and end with concluding remarks in Section V.

II. Control Law

A. Motor Model

Any ferrous particle in the strong static field of an MRI becomes magnetized, and the magnetization magnitude asymptotically approaches the saturation magnetization $\mathbf{M}_s$ of the material. The magnetic field, $\mathbf{B}_g(t)$, generated by the gradient coils, exerts a force on the ferrous particle of

$$\mathbf{F}(t) = v\,(\mathbf{M}_s \cdot \nabla)\,\mathbf{B}_g(t). \tag{1}$$

Here v is the magnetic volume of the material and $\mathbf{M}_s$ is the saturated magnetization per unit volume of the material. The magnetic field $\mathbf{B}_g(t)$ is designed to produce three independent gradients

$$[F_x, F_y, F_z]^\intercal(t) = v\mathbf{M}_{sz}\left[\frac{\partial B_{gx}}{\partial z}, \frac{\partial B_{gy}}{\partial z}, \frac{\partial B_{gz}}{\partial z}\right]^\intercal(t) \tag{2}$$

These gradients apply three independent forces on any ferromagnetic spheres inside the MRI.

See the schematic in Fig. 2. We construct rotors that constrain the ith ferromagnetic sphere to rotate about an axis $\mathbf{a}_i$ with a moment arm of length r_i. We describe the rotor's configuration by its angular position and velocity $q = [\theta_i, \dot{\theta}_i]^\intercal$. The configuration space of all n rotors is $\mathbb{R}^{2\times n}$, and the dynamic equations are given by

$$J_i\ddot{\theta}_i(t) = -b_i\dot{\theta}_i(t) - T_{f_i} - T_{l_i} + r_i\mathbf{F} \cdot \mathbf{p}_i(t) \tag{3}$$

Here J_i is the moment of inertia, b_i the coefficient of viscous friction, T_{f_i} the summation of all non-viscous friction terms seen by the input, T_{l_i} the load torque, and $\mathbf{p}_i(t)$ a vector perpendicular to $\mathbf{a}_i$ along the current direction of positive angular velocity. Actuator torque is maximized when

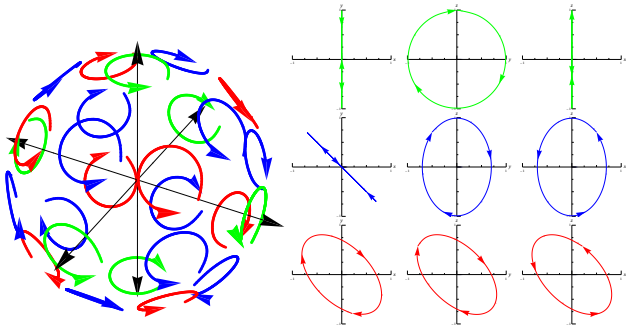

Fig. 3. The open loop control law for three orthogonal axes, (4), has 27 possible outputs corresponding with only one rotor spinning (green: turning about coordinate axis), two rotors spinning (blue), all three spinning (red), or none spinning. At right are projections onto the three coordinate axes.

$\mathbf{F}(t) = g_M V \mathbf{M}_s \operatorname{signum}(\mathbf{p}_i(t))$, where g_M is the maximum gradient.

Given $q(0) \in \mathbb{R}^{2\times n}$, and $\boldsymbol{\theta}_{\text{goal}} \in \mathbb{R}^n$ the position control problem is to find inputs $\mathbf{F}(t)$ such that for any $q(0)$ and q_{goal},

$$\lim_{t\to\infty} \sum_{i=1}^{n} \left\| \begin{bmatrix} \theta_i(t) \\ \dot{\theta}_i(t) \end{bmatrix} - \begin{bmatrix} \theta_{\text{goal},i} \\ 0 \end{bmatrix} \right\|_2 = 0.$$

We will start with the simpler velocity control problem

$$\lim_{t\to\infty} \sum_{i=1}^{n} \left\| \dot{\theta}_i(t) - \omega_i \right\|_2 = 0,$$

where $\omega_i \in \mathbb{R}$ is the desired angular velocity of each rotor. After solving the velocity control problem in Sec. II-C, we will implement an outer control loop to stabilize position in II-D.

B. Open-Loop

One method for independent control of multiple rotors using the global magnetic gradient field is to make the rotors revolve around orthogonal axes. For notational simplicity, we will assume rotors rotate about the world x, y, z axes. With $n \leq 3$ orthogonal rotors, we can use open-loop control signals to rotate some rotors at constant velocities, and move the remaining rotors to steady-state positions. For instance, the control sequence

$$\nabla \mathbf{B}_g(t) = g_M\,[\cos(t), \sin(t), 0]^\intercal$$

rotates the z-axis rotor in the positive direction at 1 rad/s and places the x and y rotors in steady-state positions.

To rotate up to three orthogonal rotors we can rotate our magnetic field at angular frequency ω around the vector $\mathbf{a} = \frac{[a_x, a_y, a_z]^\intercal}{\sqrt{a_x^2 + a_y^2 + a_z^2}}$, where $a_i \in \{-1, 0, 1\}$ is the desired rotation of the ith axis. This gives the control law

$$\nabla \mathbf{B}_g(t) = g_M R_{\mathbf{a},\omega t} \cdot \mathbf{a}_\perp. \tag{4}$$

Here $\mathbf{a}_\perp$ is a vector perpendicular to $\mathbf{a}$ and $R_{\mathbf{a},\omega t}$ is the rotation matrix that rotates the angle ωt about the axis $\mathbf{a}$.

C. Control-Lyapunov Function

Open-loop control laws are not robust to disturbances. Under control law (4), disturbances cause the rotors to slip and skip rotations, or add oscillations to the rotors that should be stationary. Additionally, open-loop control is limited to no more than three rotors because the rotors must be mutually orthogonal. To enable robust, multi-axis control we will implement a closed-loop controller designed by a control-Lyapunov function [5]. This control law sets the three magnetic gradients to decrease the sum squared velocity error. There are configurations where no combination of velocity gradients will decrease the error, but we can always apply a non-zero gradient without increasing the sum squared error, and move the rotors to a new configuration where we can decrease the error. This control is inspired by work on controlling many mobile robots with a uniform control signal [6]. In our analysis, we will start with a simplified form of the rotor dynamics:

$$\ddot{\theta}_i(t) = \frac{r_i}{J_i}\mathbf{F}(t)\cdot\mathbf{p}_i(t) \tag{5}$$

We will add in the full dynamic model (3) later:

Given n non-parallel rotors and desired angular velocities v_i, a suitable Lyapunov function is the mean squared velocity error:

$$\begin{aligned} V(\boldsymbol{\theta},\dot{\boldsymbol{\theta}},t) &= \frac{1}{2}\sum_{i=1}^{n}\Big(\omega_i - \dot{\theta}_i(t)\Big)^2 \\ \dot{V}(\boldsymbol{\theta},\dot{\boldsymbol{\theta}},t) &= \sum_{i=1}^{n}\Big(\omega_i - \dot{\theta}_i(t)\Big)\ddot{\theta}_i(t) \\ &= \mathbf{F}(t)\cdot\sum_{i=1}^{n}\Big(\omega_i - \dot{\theta}_i(t)\Big)\frac{r_i}{J_i}\mathbf{p}_i(t) \end{aligned} \tag{6}$$

We note that $V(\boldsymbol{\theta},\dot{\boldsymbol{\theta}},t)$ is positive definite, zero only at the target velocity, and radially unbounded. We will now design a control policy such that $V(\boldsymbol{\theta},\dot{\boldsymbol{\theta}},t)\equiv\mathbf{0}$ only at the desired velocity $\boldsymbol{\theta}=\boldsymbol{\omega}$.

To make $\dot{V}(\boldsymbol{\theta},\dot{\boldsymbol{\theta}},t)$ negative semi-definite, we choose

$$\mathbf{F}(t) = g_M v \mathbf{M}_s \operatorname{signum}\left(-\sum_{i=1}^{n}\Big(\omega_i - \dot{\theta}_i(t)\Big)\frac{r_i}{J_i}\mathbf{p}_i(t)\right) \tag{7}$$

For such an $\mathbf{F}(t)$,

$$\dot{V}(\boldsymbol{\theta},\dot{\boldsymbol{\theta}},t) = -\left(\sum_{i=1}^{n}\Big(\omega_i - \dot{\theta}_i(t)\Big)\frac{r_i}{J_i}\mathbf{p}_i(t)\right)^2.$$

Notice that $\dot{V}(\boldsymbol{\theta},\dot{\boldsymbol{\theta}},t)\leq 0$, but there exists a subspace of $[\boldsymbol{\theta},\dot{\boldsymbol{\theta}}]^\intercal$ where $\dot{V}(\boldsymbol{\theta},\dot{\boldsymbol{\theta}},t)=0$. Because this derivative is negative semi-definite, we can only claim stability, not asymptotic stability. To gain a proof of asymptotic stability, we must prove the invariant set contains only the rotors moving at the desired angular velocity.

We modify (7) as follows:

$$\begin{aligned} \mathbf{f} &= \operatorname{signum}\left(-\sum_{i=1}^{n}\Big(\omega_i - \dot{\theta}_i(t)\Big)\frac{r_i}{J_i}\mathbf{p}_i(t)\right) \\ \mathbf{F}(t) &= g_M v \mathbf{M}_s \begin{cases} [1,1,1]^\intercal & \text{if } \mathbf{f}=0 \text{ and } \dot{\boldsymbol{\theta}}\neq\boldsymbol{\omega} \\ \mathbf{f} & \text{else} \end{cases} \end{aligned} \tag{8}$$

This ensures that the only invariant state is the target velocity $\dot{\boldsymbol{\theta}}=\boldsymbol{\omega}$. At all other configurations where $\dot{V}(\boldsymbol{\theta},\dot{\boldsymbol{\theta}},t)=0$, the control law (8) generates a nonzero acceleration $\ddot{\theta}_i(t)$ without increasing $V(\boldsymbol{\theta},\dot{\boldsymbol{\theta}},t)$, and thus some rotors will change velocities.

D. Position Control

We can wrap a position control loop around (8) with a time-varying $\boldsymbol{\omega}$. insert control law and discussion

III. Analysis

Using multiple rotors simultaneously in the same MR scanner introduces challenges not seen with only one rotor. In this section we analyze the magnetic interaction between the ferrous spheres, interference when imaging, and questions about the optimal placement of the rotors.

A. Minimum separation between ferrous components

Any ferrous material placed in the 3 T magnetic field of a MR scanner becomes strongly magnetized and is a strong magnetic dipole. With two MR-powered motors, these dipoles exert forces on each other. This section examines the minimum separation required between each rotor.

The magnetic field at position $\mathbf{r}_2$ generated by a spherical magnet at position $\mathbf{r}_1$ with magnetization $\mathbf{m}_1$ is given by [7]

$$\mathbf{B}_{\mathbf{r}_1}(\mathbf{r_2}) = \frac{\mu_0}{4\pi}\frac{3\mathbf{n}_{12}(\mathbf{n}_{12}\cdot\mathbf{m}_1)-\mathbf{m}_1}{|\mathbf{r}_2-\mathbf{r}_1|^3} \tag{9}$$

With $\mathbf{n}_{12}=(\mathbf{r}_2-\mathbf{r}_1)/|\mathbf{r}_2-\mathbf{r}_1|$. This is the *magnetic field of a dipole*. The force applied to a dipole at $\mathbf{r}_1$ with magnetic moment $\mathbf{m}_1$ by another dipole at $\mathbf{r}_2$ with magnetic moment $\mathbf{m}_2$ is, to a low order Taylor-series expansion,

$$\begin{aligned} \mathbf{F}_{12} = \frac{\mu_0}{4\pi}\frac{1}{|\mathbf{r}_2-\mathbf{r}_1|^4}\Big[15\mathbf{n}_{12}\Big(&(\mathbf{m}_1\cdot\mathbf{n}_{12})(\mathbf{m}_2\cdot\mathbf{n}_{12})\Big) \\ -3\mathbf{n}_{12}(\mathbf{m}_2\cdot\mathbf{m}_1) - 3\Big(&\mathbf{m}_1(\mathbf{m}_2\cdot\mathbf{n}_{12})+\mathbf{m}_2(\mathbf{m}_1\cdot\mathbf{n}_{12})\Big)\Big] \end{aligned} \tag{10}$$

Figure 4 shows contour plots for the magnetic force exerted by two identical spheres on each other. The contour lines are drawn at $\mathbf{F}_{12}\cdot\mathbf{n}_{12} = g_M\cdot\{-1,-0.1,0,\frac{1}{10},1\}$. Rotors with spheres closer than the inner contour lines will become stuck because they experience a force greater than what the gradient can exert. The maximum force is along the z axis, and the critical distance when the attractive force becomes greater than the maximum gradient force is $z=\sqrt[4]{\frac{2\mathbf{M}_s\mu_0 r^3}{g_M}}$.

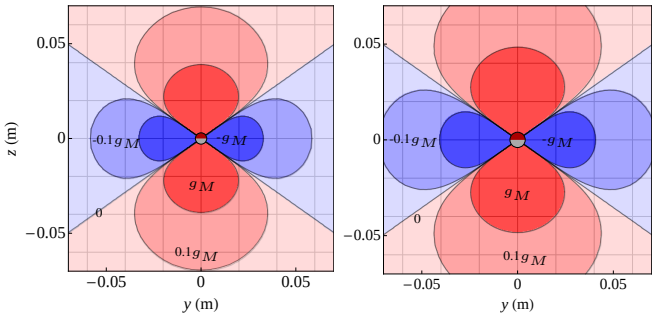

Fig. 4. One ferrous sphere in a 3T magnetic field exerts a force $\mathbf{F}$ on an identical sphere. The contour lines show $\mathbf{F} \cdot \mathbf{n}_{12}$, the force component radially outward from the sphere at $(0, 0)$ compared to the maximum force provided by the gradient coils g_M. This force is attractive (red) along the z axis and repulsive (blue) perpendicular to z. The magnetic field is symmetric about the z axis. If two spheres move within the dark red region, they cannot be separated using the gradient field. (left: 3 mm radius, right 4 mm radius spheres)

B. *Feedback Sensing*

An MR scanner can provide both power and feedback sensing for closed-loop motor control. Though ferrous particles cannot be imaged with an MR scanner, we can detect their location by detecting the sensor shadow

-image showing 3 rotors, and the x and y scans

(?) image showing that the peaks flatten at high velocities(?)

((((OUAJDI's SECTION))))

C. *Optimal placement of n non-parallel rotors*

To control multiple rotors, our controller exploits inhomogeneity in the axes of rotation of the motor rotors. This independence is maximized when the axes' orientations are *well-spaced*, that is all axes are as far from being parallel as possible. Because the rotors will be used in the uniform gradient field of an MRI, their physical location is not important, as long as we respect the dipole forces described in Sec. łsubsec:minimumseparation. Instead, we want to generate vector axes of rotation consisting of the unit vectors $\mathbf{a}_1, \mathbf{a}_2, \ldots, \mathbf{a}_n$, $\mathbf{a}_i \in \mathbb{R}^3$ that are non-parallel.

This problem is a generalization of the Thomson problem [8] that determines the minimum energy configuration for n electrons confined to the surface of a sphere. To each of the n electrons located at $\mathbf{a}_i$ we bind another electron at $-\mathbf{a}_i$, and find the minimum energy solution. As in the original Thomson problem, minimal energy configurations can be rigorously identified in only a handful of cases. Instead, as in [9], we will use numerical optimization methods to find approximately optimal solutions.

The energy

$$\begin{aligned} &\underset{\mathbf{a}_1,\mathbf{a}_2,\ldots,\mathbf{a}_n}{\text{minimize}} \sum_{i \neq j} \frac{1}{\|\mathbf{a}_i - \mathbf{a}_j\|_2^2} + \frac{1}{\|\mathbf{a}_i + \mathbf{a}_j\|_2^2} \\ &\text{subject to } \mathbf{a}_i \in \mathbb{R}^3, \|\mathbf{a}_i\|_2 = 1,\ 1 \leq i \leq n \end{aligned} \tag{11}$$

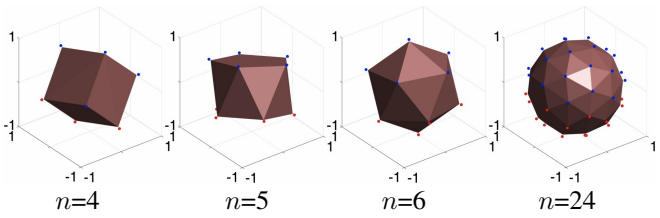

Fig. 5. Numerical optimization of rotor axes spacing for different numbers of axes n. As in the Thomson problem, minimal energy conditions have not been identified for all n. For n=2 and 3 the axes must be orthogonal. From left to right: cube, pentagonal anti prism, icosahedron, and irregular for n=24.

Both the objective function and the constraints are nonconvex. We can reformulate (11) as an unconstrained problem by changing to a spherical coordinate system parameterized by azimuth λ and elevation ϕ:

$$x = \cos(\phi)\sin(\lambda), \quad y = \cos(\phi)\cos(\lambda), \quad z = \sin(\phi).$$

The original problem had $3n$ variables and n constraints. Using spherical coordinates we have $2n$ variables and no constraints. Using the shorthand $c_\theta = \cos(\theta), s_\theta = \sin(\theta)$, we can recompute the objective function (11) as

$$\begin{aligned} f = \sum_{j=1}^{n} \sum_{i=1}^{j} &\frac{1}{2\left(1 - c_{\phi_i} c_{\phi_j} c_{\lambda_i - \lambda_j} - s_{\phi_i} s_{\phi_j}\right)} + \\ &\frac{1}{2\left(1 + c_{\phi_i} c_{\phi_j} c_{\lambda_i - \lambda_j} + s_{\phi_i} s_{\phi_j}\right)} \end{aligned} \tag{12}$$

and calculate the gradient as

$$\begin{aligned} \frac{\partial f}{\partial \phi_i} =& \frac{c_{\phi_i} c_{\lambda_i - \lambda_j} s_{\phi_i} - c_{\phi_i} s_{\phi_i}}{2\left(1 - c_{\phi_i} c_{\phi_j} c_{\lambda_i - \lambda_j} - s_{\phi_i} s_{\phi_j}\right)^2} + \\ &\frac{c_{\phi_i} c_{\lambda_i - \lambda_j} s_{\phi_i} - c_{\phi_i} s_{\phi_i}}{2\left(1 + c_{\phi_i} c_{\phi_j} c_{\lambda_i - \lambda_j} + s_{\phi_i} s_{\phi_j}\right)^2} \\ \frac{\partial f}{\partial \lambda_i} =& \frac{c_{\phi_i} c_{\phi_j} s_{\lambda_i - \lambda_j}}{2\left(1 - c_{\phi_i} c_{\phi_j} c_{\lambda_i - \lambda_j} - s_{\phi_i} s_{\lambda_j}\right)^2} + \\ &\frac{c_{\phi_i} c_{\phi_j} s_{\lambda_i - \lambda_j}}{2\left(1 + c_{\phi_i} c_{\phi_j} c_{\lambda_i - \lambda_j} + s_{\phi_i} s_{\lambda_j}\right)^2}. \end{aligned} \tag{13}$$

We find locally optimal solutions using gradient descent on (12) and (13). Our MATLAB code implementing this optimization is available at [10].

D. *Torque as a Function of n*

The MRI gradient field is unaffected by the presence of multiple rotors, so we can scale our torque linearly by adding multiple axis-aligned rotors. If we want to control these rotors independently, we must introduce inhomogeneity. By orienting the rotors along different axis of rotation we will still generate a larger sum torque, but the gain is sublinear in the number of rotors because the rotors are not necessarily aligned. In this section we analyze the torque produced with 1, 2, 3 or n rotors.

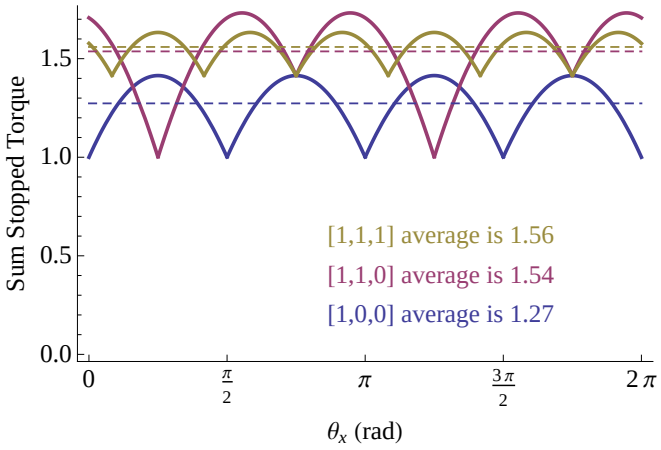

Fig. 6. With one rotor that rotates about one magnetic-field axis, the average stopped torque is $\frac{4}{\pi}$, with minimum 1 and maximum $\sqrt{2}$. By rotating about the vector $[1, 1, 0]$ or $[1, 1, 1]$ we can generate slightly larger average torques.

a) 1 rotor: Consider one rotor aligned along the MRI x-axis. The state is $[\theta_x, \dot{\theta}_x]^\intercal$. Actuating the F_y and F_z gradient fields will impart a torque on this rotor. For ease of analysis we will compare the *stopped torque*, the torque applied to a stationary rotor. Without loss of generality, we will assume that the velocity error is +1, and evaluate our control law (7) as a function of θ_x. After setting the max gradient, rotor length, saturation magnetization, and inertia to 1, the output torque is

$$T_x = -\operatorname{signum}(-c_{\theta_x})\, c_{\theta_x} + \operatorname{signum}(s_{\theta_x})\, s_{\theta_x} \tag{14}$$

Integrating (14) over θ_x produces an average torque of $\frac{4}{\pi} \approx 1.56$ Nm. Equation (14) is plotted in Fig. 6. Note that a rotor spinning around the axis [1,1,0] or [1,1,1] generates slightly larger average torques than [1,0,0].

b) 2 rotors: With two orthogonal rotors oriented along the MRI x and y axis, the sum stopped torque averaged over every rotor angle is $\frac{2(2+\pi)}{\pi^2} \approx 2.08$, and each rotor torque averages $\frac{2+\pi}{\pi^2} \approx 1.04$. For a nonzero error velocity a nonzero torque will be applied, however there are configurations where the sum torque is zero, as shown in Fig. 7. The minimum sum torque is 0 and the maximum is $2\sqrt{2} \approx 2.83$.

c) 3 rotors: With three orthogonal rotors oriented along the MRI x, y, and z axis, the sum stopped torque averaged over every rotor angle is $\frac{24}{\pi^2} \approx 2.43$, and each rotor torque averages $\frac{8}{\pi^2} \approx 0.81$. The three torques produced are

$$\begin{aligned}
\tau_x &= \operatorname{signum}(-c_{\theta_x} + s_{\theta_y}) c_{\theta_x} - \operatorname{signum}(-c_{\theta_z} + s_{\theta_x}) s_{\theta_x} \\
\tau_y &= \operatorname{signum}(-c_{\theta_y} + s_{\theta_z}) c_{\theta_y} - \operatorname{signum}(-c_{\theta_x} + s_{\theta_y}) s_{\theta_y} \\
\tau_z &= \operatorname{signum}(-c_{\theta_z} + s_{\theta_x}) c_{\theta_z} - \operatorname{signum}(-c_{\theta_y} + s_{\theta_z}) s_{\theta_z} \\
\frac{24}{\pi^2} &= \frac{1}{(2\pi)^2} \int_0^{2\pi}\int_0^{2\pi}\int_0^{2\pi} \tau_x + \tau_y + \tau_z \, \mathrm{d}\theta_x \, \mathrm{d}\theta_y \, \mathrm{d}\theta_z.
\end{aligned} \tag{15}$$

d) n-rotors: With n rotors aligned at arbitrary axis, we can calculate the average sum stopped torque by integrating over each DOF:

$$\frac{1}{(2\pi)^n} \underbrace{\int_0^{2\pi} \cdots \int_0^{2\pi}}_{n} \sum_{i=1}^{n} \tau_i + \, \mathrm{d}\theta_1 \ldots \, \mathrm{d}\theta_n \tag{16}$$

In practice, this integral is difficult to evaluate, so we use Monte Carlo simulations to estimate the quantity. Every data point in Fig. 8 is the result of 10^6 simulations. We simulated three methods for orienting our rotors:

- *Optimized:* using the numerical optimization from Section III-C we generate the largest average stopped torque and the lowest variance.
- *Random:* in spherical coordinates, we set the azimuth and orientation of the rotor axis uniformly randomly in [0,1]. This setup produces lower average torque and larger, erratic variance values than the optimized rotor axes
- *All z-axis:* sets all rotor axis to [0,0,1]. This setup has no inhomogeneity. However, the system is controllable as long as the rotors have different initial orientations: $\theta_i(0) \neq \theta_j(0)\ \forall i, j \in [1, n]$. This method results in the lowest average torque and the largest variance values.

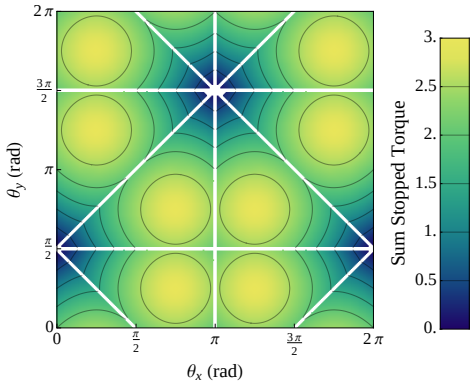

Fig. 7. The average total torque with two orthogonal rotors spinning about $[1, 0, 0]$ and $[0, 1, 0]$ is ≈2.08. The individual torques average ≈1.04.

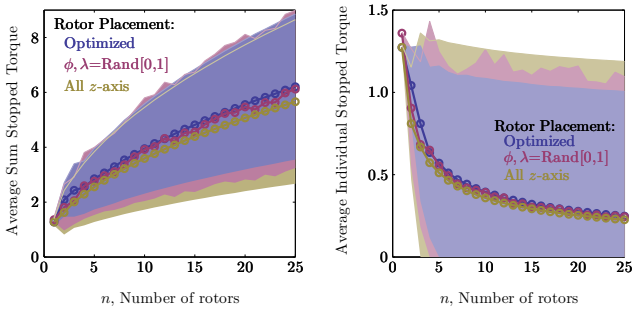

Fig. 8. Average stopped torque as a function of the number of rotors n for three different axes placement strategies. The sum torque increases sublinearly with n. The scale is normalized so 1 is the maximum torque a single gradient could impart on one rotor. Mean and ±one standard deviation are plotted. The *optimized* placement strategy has the highest average torque and lowest variance.

IV. Experiment

A. Open-loop control of multiple orthogonal rotors

plot from MRI, showing position of 3 rotors that are orthogonal. Use control law (4)

B. Simultaneous Tracking of multiple rotors

plot from MRI

C. Simulations with n rotors

1) Velocity Control:

plot with 3 rotors, with 30 rotors

2) Position Control:

plot with 3 rotors, with 30 rotors

3) Holding Torque:

plot with maximum T_ℓ load with 1,2,5,10,30 rotors, plot of rise time for one of these

V. Conclusion and Future Work

This paper has focused on control-theoretic challenges for controlling many rotors with the same, shared magnetic field from a MR scanner. In this work we *(1)* provided a globally asymptotically stabilizing controller for n actuators powered and controlled by the global magnetic field of a clinical MRI scanner *(2)* provided an optimization scheme for rotor placement

Many challenges remain. Our control scheme requires accurate state estimation. One technique is to use MRI fiducials mounted on the rotor shaft to measure the current θ_i angle of each rotor, as in [11]. Fast tracking sequences introduce a non-trivial data-association problem, which we partially addressed in Sec. III-B. Unfortunately the MRI cannot sense and actuate simultaneously, so this method requires time-multiplexing between sensing and actuation. Each sensing cycle requires 26 ms, so even a low sensing rate of 10 Hz requires 1/4 of the duty cycle, during which the motor does not produce torque. Such low sensing rates make reliable angular velocity estimation infeasible. A more promising avenue is to use an external camera and a fiducial attached to the rotor, as in [CITE]. A commercial camera with a large lens can be placed safely far from the MRI bore and measure the current rotor position with low latencies. The system would remain tetherless, MR-safe, and avoids injecting MR artifacts, but requires an unobstructed view of the motors. We are investigating methods to share camera data with the MRI control computer.

We designed our system to exploit inhomogeneities in rotor axes orientation. Constructing motors with axes that are not parallel requires careful balancing of the rotor shafts. However, it is not necessary for the rotors to be non-parallel. In simulations, control law (8) allowed controlling many rotors using other inhomogeneities, e.q. $r_i, \theta_i(0), v$. If all the axes are parallel to the gravity vector, gravity no longer interferes with rotor movement. This makes counterweights unnecessary, and allows the use of extremely low-friction vee jewel bearings because the shafts are not under radial load.

Finally, the methods presented in this paper enable simultaneous control of multiple MRI-powered motors. We are inspired by the three-axis needle driving robot of Walsh [12], designed to be used with CT scanners. A similar system, with three MRI-powered actuators, could provide low-cost robotic image-guided biopsy inside the MRI bore.

VI. Acknowledgements

This work was supported by the National Science Foundation under NRI-1208509.

References

[1] M. A. Guttman, P. Kellman, A. J. Dick, R. J. Lederman, and E. R. McVeigh, "Real-time accelerated interactive MRI with adaptive TSENSE and UNFOLD," *Magnetic Resonance in Medicine*, vol. 50, no. 2, pp. 315–321, 2003.

[2] M. Li, A. Kapoor, D. Mazilu, and K. A. Horvath, "Pneumatic actuated robotic assistant system for aortic valve replacement under mri guidance," *Biomedical Engineering, IEEE Transactions on*, vol. 58, no. 2, pp. 443–451, 2011.

[3] P. Vartholomeos, L. Qin, and P. E. Dupont, "MRI-powered actuators for robotic interventions," in *IEEE Int. Rob. and Sys.*, 2011, pp. 4508–4515.

[4] P. Vartholomeos, C. Bergeles, L. Qin, and P. E. Dupont, "An mri-powered and controlled actuator technology for tetherless robotic interventions," *Int. J. Rob. Res.*, vol. 32, no. 13, pp. 1536–1552, 2013.

[5] Z. Artstein, "Stabilization with relaxed controls," *Nonlinear Analysis*, vol. 15, no. 11, pp. 1163–1170, 1983.

[6] A. Becker, C. Onyuksel, and T. Bretl, "Feedback control of many differential-drive robots with uniform control inputs," in *IEEE/RSJ International Conference on Intelligent Robots and Systems (IROS)*, Oct. 2012.

[7] B. Thomaszewski, A. Gumann, S. Pabst, and W. Straßer, "Magnets in motion," *ACM Transactions on Graphics (TOG)*, vol. 27, no. 5, p. 162, 2008.

[8] J. J. Thomson, "On the structure of the atom: an investigation of the stability and periods of oscillation of a number of corpuscles arranged at equal intervals around the circumference of a circle; with application of the results to the theory of atomic structure," *Philosophical Magazine Series 6*, vol. 7, no. 39, pp. 237—265, Mar. 1904.

[9] H. Peng and Y. Yu, "Optimization on the surface of the (hyper)-sphere," Purdue University, Tech. Rep., May 2012. [Online]. Available: https://www.cs.purdue.edu/homes/pengh/reports/590OP.pdf

[10] A. Becker. (2013, Nov.) "Generate Non-Parallel Axes." MATLAB Central File Exchange. [Online]. Available: http://www.mathworks.com/matlabcentral/fileexchange/44515

[11] C. Bergeles, P. Vartholomeos, L. Qin, and P. E. Dupont, "Closed-loop commutation control of an mri-powered robot actuator," in *IEEE International Conference on Robotics and Automation*, May 2013, pp. 690–695.

[12] C. J. Walsh, "Image-guided robots for dot-matrix tumor ablation," Ph.D. dissertation, Massachusetts Institute of Technology, Massachusetts Institute of Technology. Dept. of Mechanical Engineering., 2010. [Online]. Available: http://hdl.handle.net/1721.1/61613